ORIGINAL PAPER

The use of Fe$_3$O$_4$/MnO$_2$-Ag nano-photocatalyst to remove dyes from real wastewater samples under visible light

H. Pouresmaeil[1] · G. R. Nabi Bidhendi[1]

Abstract

There are many challenges to advance the industrial applications of photocatalysts such as the difficulty of using ultraviolet waves in the photocatalyst applications. The present paper aims to evaluate the use of Ag additive on the photocatalyst degradation efficiency of Fe$_3$O$_4$/MnO$_2$ in the case of a real wastewater sample. In this study, Fe$_3$O$_4$/MnO$_2$-Ag nano-photocatalyst is synthesized and utilized for the removal of dyes from real wastewater under visible light. In this regard, important variables including pH, COD (as an index of dye concentration), Ag amount, and the amount of photocatalyst usage were concerned. For evaluating the microstructure and purity of the synthesized photocatalyst, TEM, SEM, FESEM, XRD, and EDS analysis were utilized. Response Surface Methodology (RSM) was applied to designing the experiments, evaluating the interaction effects, and optimizing the process factors by using Design Expert software V3 software. Based on ANOVA results, the high predictive capability of the utilized model was confirmed. The results of analysis and experiments demonstrated that, based on TEM and SEM micrographs, the nanocomposite consists of semi-spherical Fe$_3$O$_4$ particles with a clear MnO$_2$ layer. In addition, the synthesized Fe$_3$O$_4$/MnO$_2$-Ag nano-photocatalyst showed to have suitable optical and photocatalysis properties. In addition, it exhibited high photocatalytic activity, with an efficiency of more than 80% even after 6 consecutive runs. In addition, the use of Ag enhanced the photocatalytic performance and contributed to the good recovery capability of the nanocomposite.

Keywords Fe$_3$O$_4$/MnO$_2$-Ag · Nanocomposite · Photocatalysis · Wastewater treatment · Stability analysis · Response surface methodology (RSM) · Dyes degradation · Recovery capability

Introduction

In recent years, water supplies have faced critical conditions (Gheibi et al. 2021). Due to their non-biodegradable nature, dyes and other organic pollutants are known as significant hazards to the environment and human health (Al-Tohamy et al. 2022; Lellis et al. 2019). The increasing trend of industries related to textile and dyeing has resulted in massive amounts of wastewater containing residual dyes (Yaseen and Scholz 2019). Traditional wastewater treatment methods often proved to be very costly and ineffective in removing such pollutants and the recovery of energy and water in the case of wastewater

plants is highly suggested (Nasim et al. 2021; Pouresmaeil et al. 2022). In the literature, to remove dyes from wastewater, many approaches have been suggested such as physical, chemical, and biological methods (Bal and Thakur 2022). From these approaches, the photocatalysis method was determined to have great economic and efficiency potential (Fierascu et al. 2023).

Tabrizi Hafez Moghaddas et al. (2020) synthesized the green pure zinc oxide (ZnO) nanoparticles (NPs) for the photocatalytic degradation of methylene blue and demonstrated that the presence of uniform ZnO (25 nm) led to removing 80% of methylene blue within 2 h. Jasrotia et al. (2022) provided copper-modified zinc-magnesium nanoferrites for degrading dyes and demonstrated a great degradation efficiency and easy separation. In (Neelgund and Oki 2020), researchers synthesized ZnO nanocomposite onto graphene nanosheets and demonstrated a proper degradation of the anionic dye methyl orange compared to cationic dyes. Abhilash et al. (2019) synthesized the

Fe_2O_3/Cu_2O nanocomposite and found that the morphology, and structure of the synthesized nanocomposite were size-dependent and can be controlled by temperature variations in the process of synthesis. They showed that the mentioned nanocomposite had excellent photocatalytic activity, degrading model dyes Rhodamine-B and Janus green. Chankhanittha et al. (2020) introduced Bi_2MoO_6 as a great catalyst and demonstrated 90% efficiency in photodegrading of two different azo dyes. Balu et al. (2019) presented a procedure to synthesize a novel ternary Z-scheme photocatalyst namely g-C_3N_4/ZnO@α–Fe_2O_3, for organic dye degradation and introduced the potential of the ternary nanocomposite in cases of efficient organic dye degradation applications. Tran et al. (2021) also introduced $Cu_{0.5}Mg_{0.5}Fe_2O_4$–TiO_2 photocatalyst to degrade rhodamine B dye and provided outstanding results. Vinayagam et al. (2020) synthesized ZnO from the Calliandra haematocephala leaves and showed strong photocatalytic activity of degrading methylene blue dye under solar radiation. Veziroglu et al. (2020) presented a new method of synthesis to prepare a photocatalyst namely Au nanocluster (NC) decorated TiO_2 thin film, and showed that at low surface coverage, the Au NCs improved the optical absorption of TiO_2. Gandamalla et al. (2021) focused on the synthesis of a hybrid photocatalyst, $CdMoO_4$/g–C_3N_4 (CMO/CN), and demonstrated its great potential for environmental remediation and energy applications. In addition, many studies are focused on the use of graphene oxide (GO) photocatalysis to remove dyes from wastewater (Idris et al. 2021; Nguyen et al. 2021; Parthipan et al. 2021) and provided great results. As can be seen, the main focus of researchers is on the synthesis of new photocatalysis and less attention has been paid to the industrial and semi-industrial applications of these photocatalysts except for a handful of studies. Senthil et al. (2021) synthesized nano-sized AgBr-covered potato-like Ag_2MoO_4 composite photocatalysts and demonstrated that the AgBr/Ag_2MoO_4 composite as an outstanding photocatalytic material for industrial wastewater purification. However, the high price of material usages is the main deficiency of this method. Adabavazeh et al. (2020) suggested a new nanocomposite to degrade parathion under visible light and exhibited the high efficacy in the degradation of parathion from a real wastewater.

Many studies have been performed in the case of Fe_3O_4–MnO_2 applications for the redemption of wastewater. (Zhao et al. 2016) utilized Fe_3O_4–MnO_2 to remove bivalent heavy metals from aqueous systems and provided appropriate results. (Liu et al. 2015) used Fe_3O_4–MnO_2 to remove 4-chlorophenol from wastewater and the synthesized Fe_3O_4–MnO_2 showed to have very effective

structures based on microscopic analysis. Besides many applications of photocatalysts, many scholars such as (Osman et al. 2020) have suggested to use of active photocatalysts from waste materials for different applications.

Based on the method and results presented by previous researchers, many issues have not yet been resolved. The first problem is the fact that the main focus of researchers is on the synthesized wastewater in the laboratory. However, together with dyes in the wastewater, there can be many pollutions, which may affect the performance of the photocatalyst in removing dyes. In addition, many researchers concentrated on the use of expensive metals such as Au to improve the optical properties of photocatalysts that highly affected the generality of photocatalysts. Finally, despite the optical and effective properties of MnO_2, its performance has not been exanimated as a photocatalyst for dye removal from wastewater under visible wavelengths, satisfactorily, and almost all investigations are performed based on UV light. Hence, considering these issues, we have synthesized the Fe_3O_4/MnO_2 nano-photocatalysis, and its optical properties were enhanced by using silver (Ag). Ag-based semiconductors are highly suggested due to their strong visible-light absorbing capability together with small bandgap energy. The enhanced photocatalyst was then evaluated in the case of dye removal from real wastewater based on chemical oxygen demand (COD). In the following, firstly, the purchased materials and synthesis methods are briefly introduced, and then, the results obtained from material characterization methods are presented. Finally, the results of functional analysis in the case of photocatalyst performance in dye removal were demonstrated.

Materials and methods

Materials

Merck $FeCl_3$, $KMnO_4$, and $AgNO_3$ as precursors of Fe_3O_4, MnO_2, and Ag, respectively, with high purities were purchased from Beckman Coulter Commercial Enterprise Nano Particles, China. In the first step, Fe_3O_4 is synthesized by using $FeCl_3$ and ammonia under an argon atmosphere. Then, the pre-synthesized Fe_3O_4 and $KMnO_4$ are mixed to synthesize Fe_3O_4/MnO_2 mixture. Finally, $AgNO_3$ was added to the mixture contained in dispersed Fe_3O_4/MnO_2 to synthesize Fe_3O_4/MnO_2–Ag. In the following the detailed process of synthesis is presented:
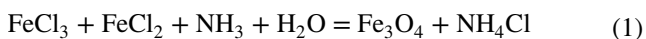
The synthesis of Fe_3O_4/MnO_2

It should be noted that the following two steps are performed, simultaneously.

Step 1: The synthesis of Fe_3O_4.

Figure shows a schematic of the setup utilized for the synthesis process. In the first step, for the synthesis of 0.5 g Fe_3O_4, 1.05 g iron chloride was added to water and placed on a magnetic stirrer at 80 °C for 1 h. Argon gas was used as a carrier gas during synthesis which prevented the oxidation of Fe_3O_4. After these stages, an orange-colored solution was formed, which demonstrated the presence of iron (II) oxide in water. Then, for changing iron (II) oxide to iron (III) oxide, ammonia was added dropwise in this solution so the solution color was turned black at room temperature for an hour. Finally, magnetite Fe_3O_4 solutions were formed. After this stage, an ultrasonic homogenizer was utilized instead of the stirrer due to the magnetic properties of iron (III) oxide. Equation (1) shows the reaction required to synthesize Fe_3O_4 (Mahmud et al. 2020). Note that the FAMCO pH meter is utilized to measure the pH of samples and 0.5 M H_2SO_4 and NH_3 are also used to adjust the pH of solutions in different stages.

$$FeCl_3 + FeCl_2 + NH_3 + H_2O = Fe_3O_4 + NH_4Cl \qquad (1)$$

Step 2: The synthesis of Fe_3O_4/MnO_2.

For the synthesis Fe_3O_4/MnO_2, when 0.5 gr Fe_3O_4 was synthesized in DI water (without the drying stage), 0.91 gr potassium permanganate ($KMnO_4$) solution was dropwise added to the mixture resulting in the formation of a dark brown suspension. Due to the magnetic behavior of the mixture, all processes of dispersing were done by an ultrasonic device using an ice water bath for 2 h during the synthesis process. After 2 h, the formed nanoparticles were collected using a magnet, washed several times with deionized water and ethanol, and then dried in an oven at a temperature of 60 °C for 12 h. Figure 1 shows a schematic of the setup utilized for the synthesis process.

Synthesis of $Fe_3O_4/MnO_2/Ag$ nanoparticles

For synthesis of the Fe_3O_4/MnO_2–Ag nanoparticles, a stoichiometric amount of Fe_3O_4/MnO_2 powder was dispersed in DI water by an ultrasonic device for half of hour. In the second stage, 55 mg $AgNO_3$ was dispersed in water and then dried at 200 °C (under a nitrogen atmosphere) to synthesize solid state Ag. After that synthesized Ag was released in the Fe_3O_4/MnO_2 solution. All of this process was performed without the addition of any extra growth-controlling agent. The obtained solution was then dispersed under ultrasonication for 2 h leading to adsorbing the Ag on the Fe_3O_4/MnO_2 surface. Afterward, the Fe_3O_4/MnO_2 was collected by using a magnet and washed with DI water to clean the excess $AgNO_3$ from the solution. Finally, the obtained powder was calcined at 400 °C and the resulting powder was washed with DI water and dried in an oven at 70 °C. Note that all processes of synthesis were performed under Ar atmosphere as a carrier
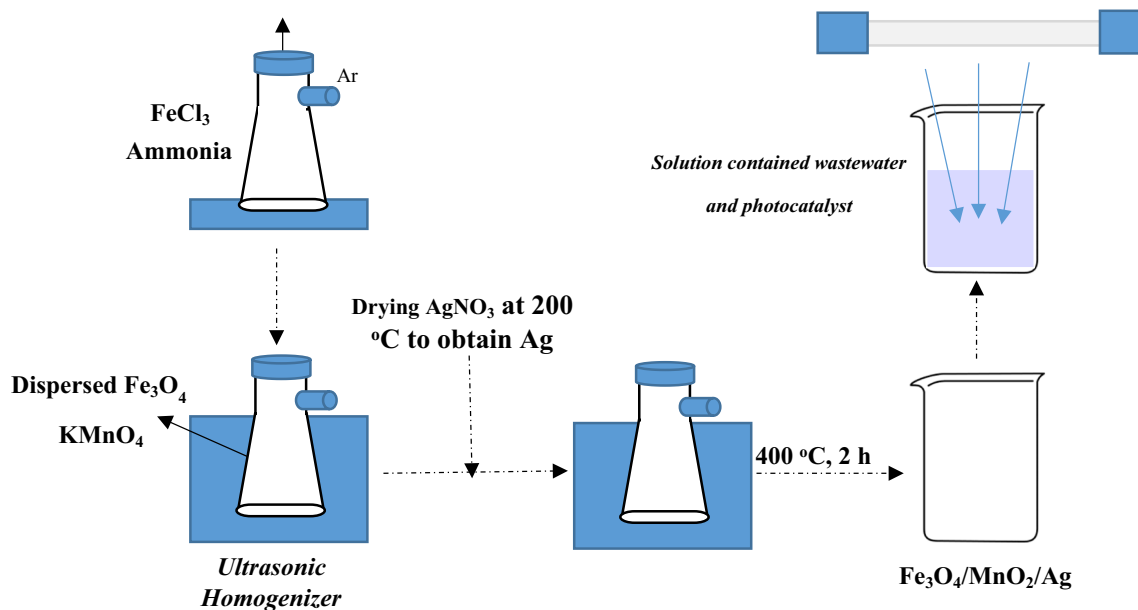

Fig. 1 The experimental setup

gas. All the process of synthesis is summarized in To measure the COD of the sample, the HACH DR 6000 spectrophotometry device is utilized. The standard range of between 100 mg/L and 900 mg/L is considered and the COD of wastewater samples are measured in the range of 20 mg/L to 3000 mg/L by using a spectrophotometer device at 600 nm 2.5 h. By dissolving a specific amount of dried Potassium Hydrogen Phthalate (KHP) at 110 °C, a series of sample solutions with specific COD concentrations are prepared in distilled water. Then, the calibration curve was plotted with a regression of 0.999, and the linear formula of the curve was obtained (Seid-Mohammadi et al. 2021).

Designing the experiment

In the present paper, the Response Surface Method (RSM) was employed as an experimental design technique known as a statistical and computational approach used for analyzing complex experiments and optimizing processes, widely. The use of RSM method can be used to study the relationship between independent and dependent variables, considering a more precise analysis of the influence of each variable on the responses and the identification of optimal conditions for the investigated process. For the design of the experiment, parameters A, B, C, and D were considered, respectively, the amount of silver (Ag), the amount of photocatalyst, the COD value, and the pH level. The purpose of the experiment was to determine the efficiency of the photocatalyst in removing the dyes from wastewater. Note that the COD of the utilized wastewater real sample was adjusted by adding dyes in water. The considered sample had different dyes namely benzene, toluene, and xylene (BTX) with a low concentration of heavy metal ions such Cr, Pb, etc. with initial pH of 8.5, COD around 500, and TDS of 9500. Hence, we controlled the COD and pH amounts by increasing the BTX amount and acid and base to investigate the effects of their concentration on the performance of the photocatalytic process. Noted that the standard COD of clean water showed to be lower than 60 ppm. For calculating the dye removal efficiency, the following relation was

$$R1 = \frac{COD_{\text{aftertreatment}} - COD_{\text{initial}}}{COD_{\text{initial}}} \times 100$$

Characterization

To characterize the synthesized materials different analyses of X-ray Diffraction (XRD) using Cu K radiation with graphite monochromator, Transmission Electron Microscopy (TEM), Scanning Electron Microscopy (SEM), Field Emission Scanning Electron Microscopy (FESEM) of the TESCAN MIRA3 model, was used for analysis the raw materials and obtained products from the reduction reaction. and Energy-Dispersive X-ray Spectroscopy (EDS) analysis. In addition, for measuring the number of water-soluble substances, a Thermo Scientific Spectrophotometer was utilized.

Results and discussion

Characterization of the synthesized photocatalyst

Figure 2 shows TEM, SEM, and FESEM images along with EDS analysis related to Fe_3O_4/ MnO_2-Ag composite. As can be seen, the Fe_3O_4 particles in the synthesized photocatalyst have a semi-spherical shape and the layer of MnO_2 around the Fe_3O_4 is also clear. In the case of the FESEM image, the semi-spherical microstructure of the produced photocatalyst is clear. However, the core–shell state was not clear in the FESEM analysis. In addition, the EDS analysis confirmed that the impurity value of the system is about 0.33% indicating the purity and quality of the synthesized photocatalyst.
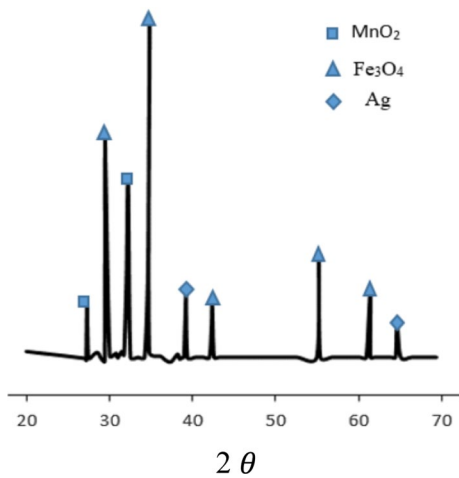
In Fig. 3, the XRD patterns are related to the synthesized Fe_3O_4/MnO_2-Ag NPs. As can be seen, there is no specific impurity but if there was, it is unlikely in an amorphous form. The high purity from the synthesis method was obtained due to controllable synthesis conditions, the formation of nano-sized particles, and the controlled and separable nature of the process. In addition, the use of high-purity precursors was also demonstrated by the utilized XRD patterns. In Fig. 3, the peaks between 25° and 45°, are related to Fe_3O_4/ MnO_2-Ag, and the sharpest peak near 35° stands for the Fe_3O_4 crystals. Based on the Scherrer equation the mean crystal size of NPs was determined to be 80 nm. Based on the Scherrer equation the mean crystal size was determined to be 84 nm. Figure 4 demonstrates the UV–visible absorption spectra related to Fe_3O_4/MnO_2 and Fe_3O_4/MnO_2-Ag nanocomposites. In comparison with the Fe_3O_4/MnO_2

Fig. 2 The SEM and TEM analysis related to Fe$_3$O$_4$/MnO$_2$-Ag

SEM **FESEM**
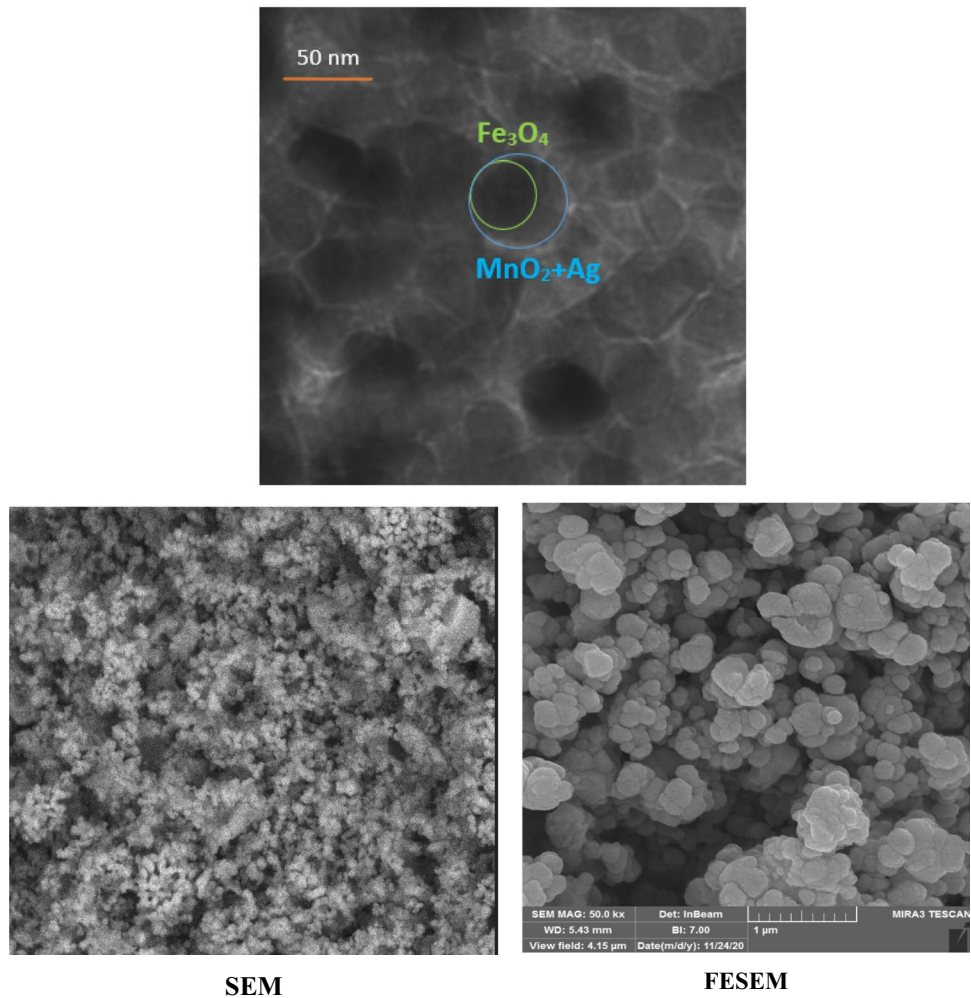
Elt	O	Fe	Mn	Ag
W%	51.23	32.89	15.54	0.33

Fig. 3 The XRD patterns related to the synthesized Fe$_3$O$_4$/ MnO$_2$-Ag NPs
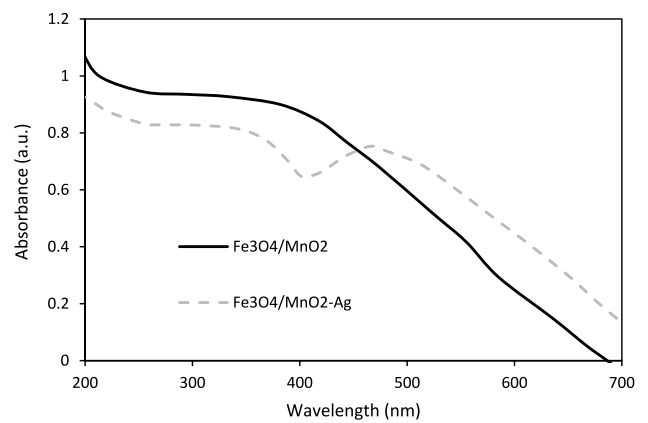
Fig. 4 The UV–visible absorption spectra related to Fe$_3$O$_4$/MnO$_2$ and Fe$_3$O$_4$/MnO$_2$-Ag nanocomposites

Table 1 The performance of photocatalysis for dye removal from real samples

Run	A: Dose (gr/lit)	B: Ag (gr)	C: COD	D: pH	R1
1	0.75	0.002	1500	3	46
2	0.5	0.002	1500	6.5	82.12
3	0.75	0.005	500	6.5	95.28
4	1	0.0035	500	6.5	98.04
5	1	0.0035	1500	10	96.88
6	0.5	0.0035	2500	6.5	87.7
7	0.75	0.0035	1500	6.5	84.94
8	0.5	0.0035	1500	3	55.09
9	0.75	0.002	500	6.5	78.84
10	0.75	0.0035	2500	10	94.17
11	0.75	0.0035	500	10	98.23
12	0.75	0.0035	2500	3	49.9
13	1	0.0035	2500	6.5	72.14
14	0.75	0.0035	500	3	54
15	0.75	0.005	1500	3	56.8
16	1	0.002	1500	6.5	67.01
17	0.75	0.005	2500	6.5	90
18	0.5	0.0035	500	6.5	84.21
19	0.75	0.0035	1500	6.5	90.33
20	0.5	0.0035	1500	10	93.08
21	0.75	0.0035	1500	6.5	90
22	0.75	0.0035	1500	6.5	91.45
23	0.75	0.002	1500	10	92.14
24	0.5	0.005	1500	6.5	82.94
25	0.75	0.0035	1500	6.5	79
26	1	0.0035	1500	3	47
27	1	0.005	1500	6.5	97.45
28	0.75	0.005	1500	10	99.9
29	0.75	0.002	2500	6.5	73.05

nanoparticles, Fe_3O_4/MnO_2-Ag demonstrated different absorption properties. Fe_3O_4/MnO_2 absorption behavior demonstrated an edge near 350 nm that can be due to the MnO_2 intrinsic band-gap absorption. In the case of Fe_3O_4/MnO_2-Ag, as can be seen, there was a new symmetric peak in the wavelengths between 400 and 500 nm attributed to the characteristic surface plasmon band of Ag NPs as mentioned in (Chidambaram et al. 2016). As a result, the possible enhancement in the photocatalysis behavior of Fe_3O_4/MnO_2-Ag compared to Fe_3O_4/MnO_2 can be due to the Surface Plasmon Resonance (SPR) property. In addition, Ag acts as an electron acceptor to gather photogenerated electrons from the surface of the photocatalyst. It also can enhance electron-hole recombination and

higher charge separation, leading to an increase in the photocatalytic activity of Fe_3O_4/MnO_2. In addition, the energy band structure of the photocatalyst can be modified by the use of Ag, enabling more effective charge transfer pathways.

The photocatalyst efficacy in the degradation of dyes

Table 1 shows the obtained results for dye removal from real samples using a photocatalyst modified with Ag under, considering different factors pH (3–10), photocatalyst dose (0.5–1 gr), COD (500–2500), and Ag amount (0.002–0.005 gr). Note that a fixed residence time was considered for all experiments (1 h) and the COD value for developing experiments was controlled by adding predicted amounts of dyes in wastewater. Noted that the design expert software V3 was utilized for the statistical analysis. Table 2 shows the variance results related to samples.

Analysis of CCD and ANOVA

In the design expert, ANOVA tables can be considered for evaluating the coefficient of each parameter as well as the related interactions. As a result, the F-value for the considered model in cases of photocatalysis degradation of dyes by using Fe_3O_4/MnO_2-Ag nano-photocatalyst was determined to be 44.97 by a P-value lower than 0.0001. It can greatly verify the practicability and its statistically of this material. The lack of Fit for the F-value and p-value was determined to be 0.9612 and 0.2615 respectively, and the software labeled it as "not significant". The fitting quality of the model was proved because of obtaining a Predicted R^2 equal to 0.9299 and an appropriate Adjusted R^2 (0.9565). Based on the obtained results, the high performance of the considered approach was confirmed in the case of a suitable prediction of experimental data. In the following, we provided the polynomial equation related to the model:

$$\begin{aligned} Y = &+ 87.14 - 0.5517A + 6.93B - 3.47C + 22.13D \\ &+ 7.41AB - 7.35AC + 2.97AD + 0.1275BC \\ &- 0.7600BD + 0.0100CD - 1.95A^{2s} - 2.21B^2 \\ &- 0.4591C^2 - 12.01D^2 \end{aligned}$$

Figure 5 shows the obtained experimental results against predicted data related to the photocatalytic

Table 2 Analysis of variance of samples

Source	Sum of squares	df	Mean square	F-value	p-value	
Model	8034.56	14	573.90	44.97	<0.0001	Significant
A-Dose	3.65	1	3.65	0.2862	0.6011	
B-Ag	576.99	1	576.99	45.22	<0.0001	
C-COD	144.49	1	144.49	11.32	0.0046	
D-pH	5879.06	1	5879.06	460.73	<0.0001	
AB	219.34	1	219.34	17.19	0.0010	
AC	215.94	1	215.94	16.92	0.0011	
AD	35.34	1	35.34	2.77	0.1183	
BD	2.31	1	2.31	0.1811	0.6769	
CD	0.0004	1	0.0004	0.0000	0.9956	
A^2	24.58	1	24.58	1.93	0.1869	
B^2	31.76	1	31.76	2.49	0.1370	
C^2	1.37	1	1.37	0.1071	0.7483	
D^2	934.88	1	934.88	73.26	<0.0001	
Residual	178.65	14	12.76			
Lack of fit	70.61	10	7.06	0.2615	0.9612	Not significant
Pure error	108.03	4	27.01			
Total	8213.21	28				

Source	Sequential p-value	Lack of fit P-value	Adjusted R^2	Predicted R^2	
Linear	<0.0001	0.1659	0.7714	0.7138	
2FI	0.3285	0.1724	0.7848	0.6351	
	<0.0001	0.9612	0.9565	0.9299	Suggested
Cubic	0.8827	0.8653	0.9340	0.8374	Aliased
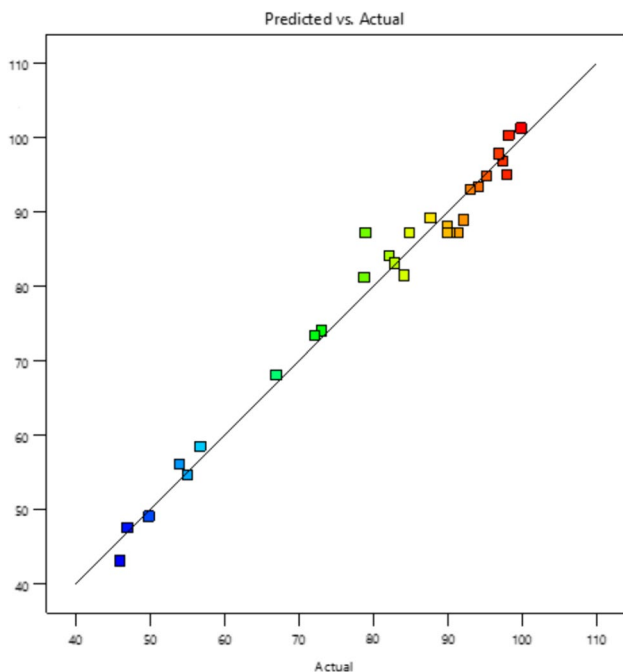
Fig.5 Experimental data vs. predicted values obtained by using the polynomial regression model

degradation of dyes based on the mentioned polynomial model. Based on Fig. 5, it was demonstrated that the rate of disagreement between experimental and predicted results was very low that another approving for the accuracy of the utilized relation for regression. Figure 6 shows response surfaces in cases of interaction between Ag amount and pH. An increase in the amount of Ag usage led to an enhancement in the optical properties of photocatalysts and performance. Figure 7 illustrates the response surface for interaction between COD and pH. As can be seen, the pH parameter, as well as the COD, can be two determinative variables in the case of photocatalytic degradation percentage. However, even at high CODs, increasing the pH value caused the degradation percentage to be increasing. At high levels of pH, the adsorption of positively charged reactants is facilitated by more negatively charged on the photocatalyst surface. In addition, the presence of increased hydroxide ions as a result of increasing pH level leads to preventing the electron–hole recombination so more electrons participate in the oxidation of dyes. As it is clear in Fig. 6, Ag
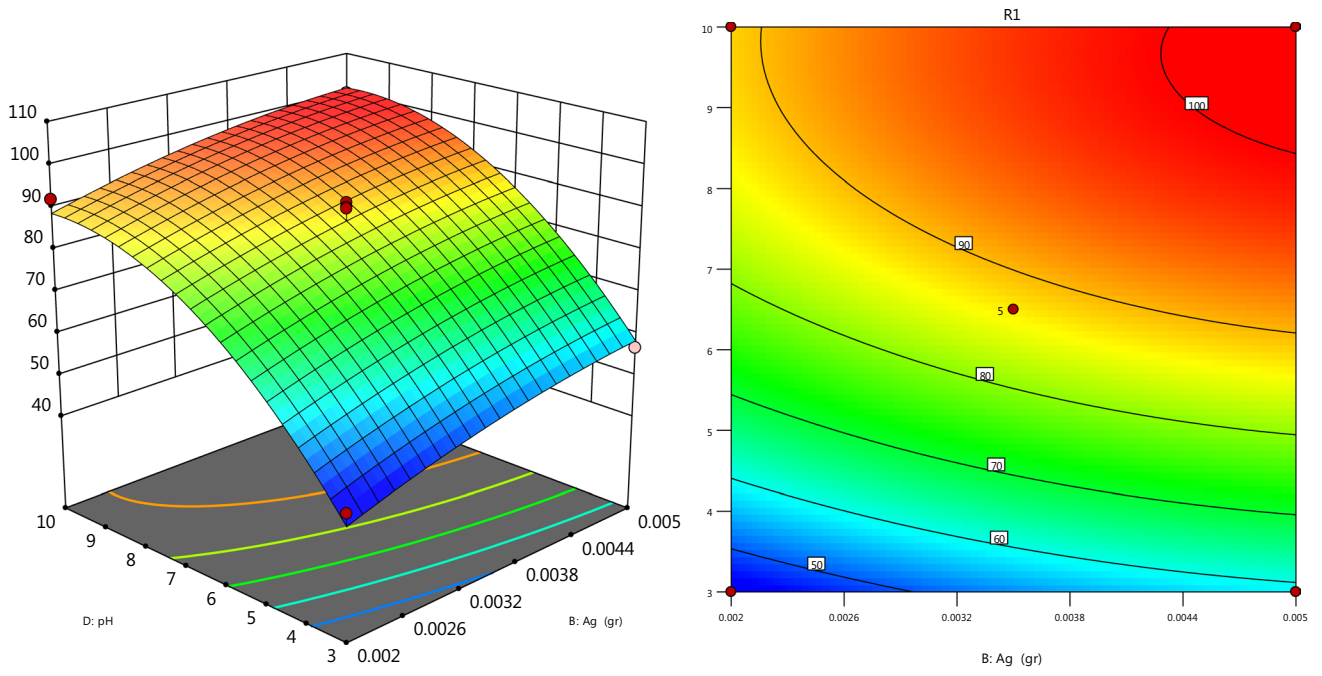
Fig. 6 The response surface for the interaction of Ag amount, pH, and R
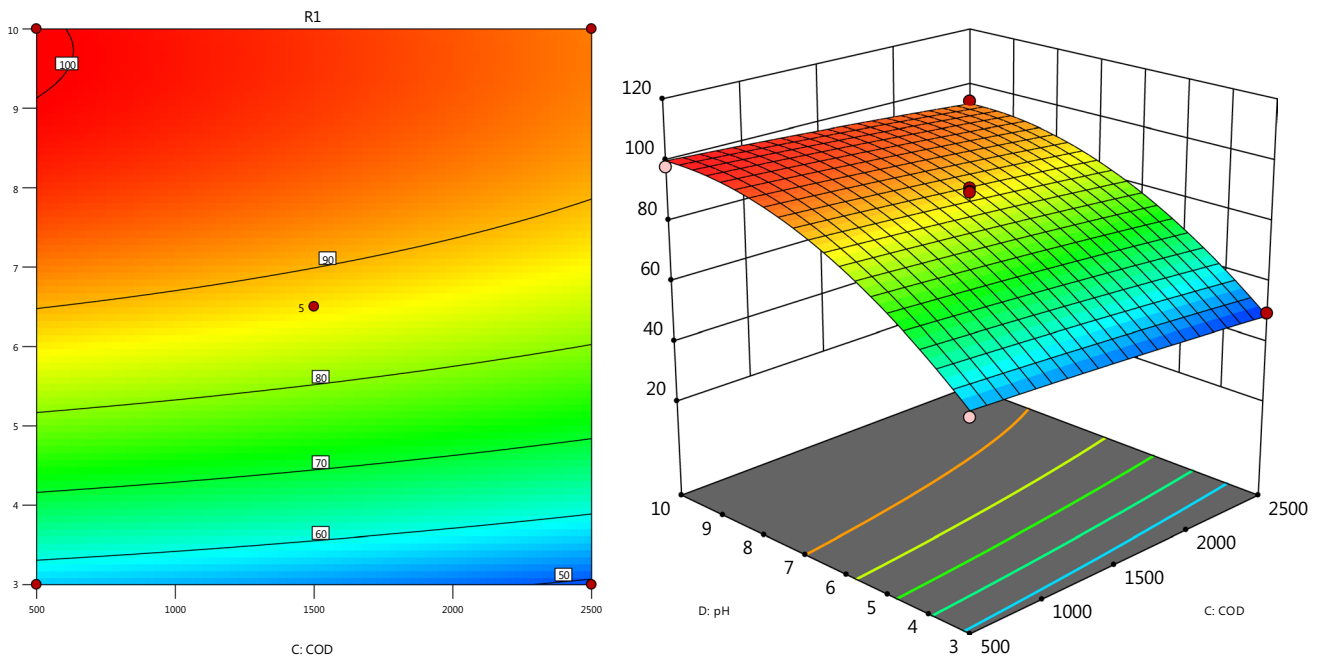

Fig. 7 The response surface of pH and COD factors on the overall photocatalyst efficiency
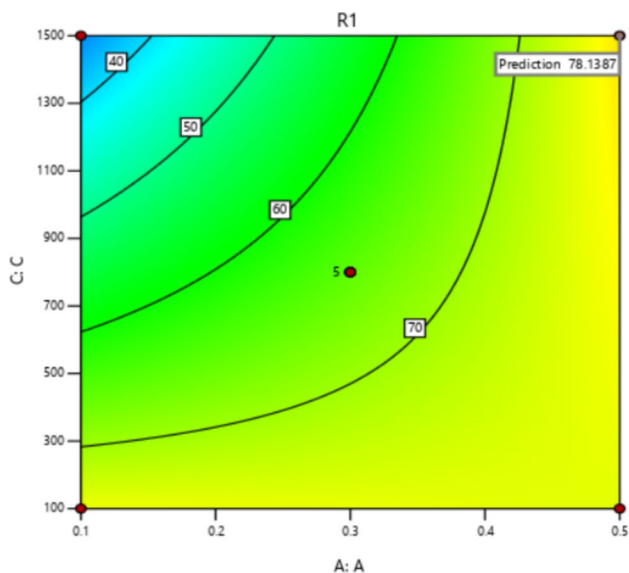
Fig. 8 The response surface of Ag and COD

Table 3 The optimized values about considered parameters

Factor	Optimized amount
A: Dose	1
B: Ag	0.5
C: COD	1500
D: pH	6.5
R1	96.77

is a very important factor in the response. Even at the pH of 7, the response is determined to be about 90% by using 0.005 gr Ag. As mentioned earlier, the use of Ag increased the band gap of the photocatalyst, and this in turn caused better absorption of waves at different wavelengths assisted in improving the photocatalytic process. Similarly, (Phu et al. 2020) found that Ag doping can considerably enhance the photocatalytic activity of the Bi_2WO_6 NPs. In (Han et al. 2020), scholars also confirmed the effective use of elements such as Cu and its outstanding results in the case of antibacterial removal efficacy against *Staphylococcus aureus*. (Abbad et al. 2020) also demonstrated the same results in the case of band-gap enhancement by using Ag and showed that the band-gap increased as a function of Ag concentration and the relation of Ag concentration on the final performance of the photocatalyst is demonstrated in the present study. The most important challenge in the field of using photocatalysts is its operational limitations in terms of the costs of using UV lamps. Based on this, the improvement of the photocatalytic process by using Ag under visible waves (which brings lower costs) is highly recommended and effective. Figure 8 shows the response surface of Ag and COD. As expected, by increasing the amount of Ag from 0.1 to 0.5 wt.% the R1 increased, significantly. However, low amounts of Ag weight percentages were determined to be unpreferable for the degradation of BTX. Table 3 shows the optimized values in the case of considered parameters obtained from the Design expert software. As can be seen, for COD of 1500, the optimized dose, Ag,

Fig. 9 The stability analysis of the synthesized Fe_3O_4/MnO_2-Ag nano-photocatalyst
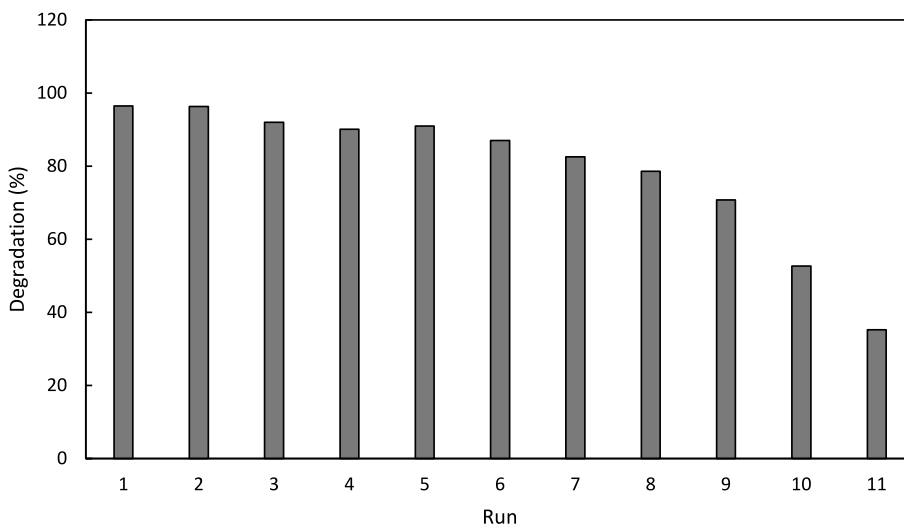
COD, and pH were determined with R1 equal to 96.77. Note that decreasing the pH value can lead to side effects such as corrosion of system pipes and increasing the pH value to around 7 can be desirable. Hence, the optimized values were chosen considering this fact.

Investigating the reusability of photocatalyst

In this section, the reusability efficiency of photocatalyst was investigated in a batch system. For each experiment, the solution contained a photocatalyst, and the wastewater was dried in an oven for 12 h at a temperature of 70 °C. Then, the resulting powder was used for the next experiment. Figure 8 shows the results from the stability analysis of the synthesized Fe_3O_4/MnO_2-Ag nanophotocatalyst evaluated utilizing 11 consecutive runs of wastewater treatment. Due to the magnetic property of the photocatalyst after each photocatalytic run, the recovering process was performed by separating the NPs from the sample using an external magnet, then these NPs were washed three times with ethanol and water then dried and prepared for the next photocatalytic run. As can be seen, even at 8 runs, the efficiency of the photocatalyst was higher than 80% which shows the very high capability of this photocatalyst in recovery. The addition of Ag to the Fe_3O_4/MnO_2 photocatalyst may have contributed to the good recovery capability of the nano-photocatalyst. As mentioned in the previous section, Ag has great catalytic properties in the oxidation processes of dyes. Incorporating Ag into the Fe_3O_4/MnO_2 photocatalyst could enhance its photocatalytic activity (Fig. 9).

Conclusion

In this study, Fe_3O_4/MnO_2-Ag nano-photocatalyst was synthesized for the removal of dyes from wastewater, and different factors of pH, COD, Ag amount, and the amount of photocatalyst were considered. The nanocomposite was characterized using TEM, FESEM, EDS, and XRD analysis and the RSM method was employed to design the experiments, analyze the interaction effects, and optimize the process factors. The ANOVA results confirmed the high predictive capability of the utilized model with R^2 of 96.77. The characterization of the synthesized Fe_3O_4/MnO_2-Ag nano-photocatalyst revealed that it consisted of semi-spherical Fe_3O_4 particles encapsulated by a clear MnO_2 layer and there are not any impurities in the synthesized photocatalysts. The high photocatalytic activity of synthesized photocatalyst was evident with efficiency exceeding 80% even after the 6th consecutive run. The addition of Ag further improved the photocatalytic performance and contributed to the good recovery capability of the nanocomposite under visible light and 0.005 gr Ag resulted in more than 90% reduction of COD. For future work, the use of a semi-industrial system based on these photocatalysts should be considered. In addition, the performance of these photocatalysts needs to be evaluated for the removal of different pollutants in water and wastewater, simultaneously.

Declarations

Conflict of interest There is no conflict of interest from the author(s).

References

Abbad S, Guergouri K, Gazaout S, Djebabra S, Zertal A, Barille R, Zaabat M (2020) Effect of silver doping on the photocatalytic activity of TiO2 nanopowders synthesized by the sol-gel route. J Environ Chem Eng 8(3):103718. https://doi.org/10.1016/j.jece.2020.103718

Abhilash MR, Akshatha G, Srikantaswamy S (2019) Photocatalytic dye degradation and biological activities of the Fe2O3/Cu2O nanocomposite. RSC Adv 9(15):8557–8568

Adabavazeh H, Saljooqi A, Shamspur T, Mostafavi A (2020) Synthesis of KIT-5 decorated by Bi2S3-Fe3O4 photocatalyst for degradation of parathion pesticide in aqueous media: Offering a degradation model and optimization using response surface methodology (RSM). Appl Organomet Chem 34(3):e5345. https://doi.org/10.1002/aoc.5345

Al-Tohamy R, Ali SS, Li F, Okasha KM, Mahmoud YAG, Elsamahy T, Jiao H, Fu Y, Sun J (2022) A critical review on the treatment of dye-containing wastewater: Ecotoxicological and health concerns of textile dyes and possible remediation approaches for environmental safety. Ecotoxicol Environ Saf 231:113160. https://doi.org/10.1016/j.ecoenv.2021.113160

Bal G, Thakur A (2022) Distinct approaches of removal of dyes from wastewater: a review. Mater Today: Proc 50:1575–1579. https://doi.org/10.1016/j.matpr.2021.09.119

Balu S, Velmurugan S, Palanisamy S, Chen S-W, Velusamy V, Yang TCK, El-Shafey E-SI (2019) Synthesis of α-Fe2O3 decorated g-C3N4/ZnO ternary Z-scheme photocatalyst for degradation of tartrazine dye in aqueous media. J Taiwan Inst Chem Eng 99:258–267. https://doi.org/10.1016/j.jtice.2019.03.011

Chankhanittha T, Somaudon V, Watcharakitti J, Piyavarakorn V, Nanan S (2020) Performance of solvothermally grown Bi2MoO6 photocatalyst toward degradation of organic azo dyes and fluoroquinolone antibiotics. Mater Lett 258:126764. https://doi.org/10.1016/j.matlet.2019.126764

Chidambaram S, Pari B, Kasi N, Muthusamy S (2016) ZnO/Ag heterostructures embedded in Fe_3O_4 nanoparticles for magnetically recoverable photocatalysis. J Alloys Compd 665:404–410. https://doi.org/10.1016/j.jallcom.2015.11.011

Fierascu RC, Fierascu I, Matei RI, Manaila-Maximean D (2023) Natural and natural-based polymers: recent developments in management of emerging pollutants. Polymers 15(9):2063. https://doi.org/10.3390/polym15092063

Gandamalla A, Manchala S, Anand P, Fu Y-P, Shanker V (2021) Development of versatile CdMoO4/g-C3N4 nanocomposite for enhanced photoelectrochemical oxygen evolution reaction and photocatalytic dye degradation applications. Materials Today Chemistry 19:100392. https://doi.org/10.1016/j.mtchem.2020.100392

Ghadami N, Siamaki M, Pouresmaeil H, Aghlmand R, Gheibi M (2021) Assessing energy consumption, optical distributions, and carbon contaminations using the design-builder simulation model (Case Study: A Sports Building, Mashhad, Iran). Annals Environ Sci Toxicol 5(1):074. https://doi.org/10.17352/aest.000040

Gheibi M, Pouresmaeil H, Akrami M, Kian Z, Takhtravan A, Mohammadi M (2021) Presenting a novel approach for designing chlorine contact reactors by combination of genetic algorithm with nonlinear condition functions, simulated annealing algorithm, pattern search algorithm and experimental efforts. Annals Environ Sci Toxicol. https://doi.org/10.17352/aest.000030

Han D, Han Y, Li J, Liu X, Yeung KWK, Zheng Y, Cui Z, Yang X, Liang Y, Li Z, Zhu S, Yuan X, Feng X, Yang C, Wu S (2020) Enhanced photocatalytic activity and photothermal effects of cu-doped metal-organic frameworks for rapid treatment of bacteria-infected wounds. Appl Catalysis b: Environ 261:118248. https://doi.org/10.1016/j.apcatb.2019.118248

Idris NJ, Bakar SA, Mohamed A, Muqoyyanah M, Othman MHD, Mamat MH, Soga T (2021) Photocatalytic performance improvement by utilizing GO_MWCNTs hybrid solution on sand/ZnO/TiO_2-based photocatalysts to degrade methylene blue dye. Environ Sci Pollut Res 28:6966–6979

Jasrotia R, Verma A, Verma R, Ahmed J, Godara SK, Kumar G, Kalia S (2022) Photocatalytic dye degradation efficiency and reusability of Cu-substituted Zn-Mg spinel nanoferrites for wastewater remediation. J Water Proces Eng 48:102865. https://doi.org/10.1016/j.jwpe.2022.102865

Lellis B, Fávaro-Polonio CZ, Pamphile JA, Polonio JC (2019) Effects of textile dyes on health and the environment and bioremediation potential of living organisms. Biotechnology Res Innovation 3(2):275–290

Liu J, Zhao Z, Shao P, Cui F (2015) Activation of peroxymonosulfate with magnetic Fe3O4–MnO2 core–shell nanocomposites for 4-chlorophenol degradation. Chem Eng J 262:854–861. https://doi.org/10.1016/j.cej.2014.10.043

Mahmud N, Nasser MS, El-Naas MH, Ba-Abbad MM, Mohammad AW, Mansour S, Benamor A (2020). Synthesis and characterization of fe_3o_4 Nanoparticles using different experimental methods. IOP Conference Series: Mater Sci Eng.

Moghaddas SMTH, Elahi B, Javanbakht V (2020) Biosynthesis of pure zinc oxide nanoparticles using Quince seed mucilage for photocatalytic dye degradation. J Alloys Compd 821:153519

Neelgund GM, Oki A (2020) ZnO conjugated graphene: an efficient sunlight driven photocatalyst for degradation of organic dyes. Mater Res Bull 129:110911. https://doi.org/10.1016/j.materresbull.2020.110911

Nguyen TKA, Pham T-T, Nguyen-Phu H, Shin EW (2021) The effect of graphitic carbon nitride precursors on the photocatalytic dye degradation of water-dispersible graphitic carbon nitride photocatalysts. Appl Surface Sci 537:148027. https://doi.org/10.1016/j.apsusc.2020.148027

Osman AI, Skillen NC, Robertson PKJ, Rooney DW, Morgan K (2020) Exploring the photocatalytic hydrogen production potential of titania doped with alumina derived from foil waste. Int J Hydrogen Energy 45(59):34494–34502. https://doi.org/10.1016/j.ijhydene.2020.02.065

Parthipan P, Cheng L, Rajasekar A, Govarthanan M, Subramania A (2021) Biologically reduced graphene oxide as a green and easily available photocatalyst for degradation of organic dyes. Environ Res 196:110983. https://doi.org/10.1016/j.envres.2021.110983

Phu ND, Hoang LH, Van Hai P, Huy TQ, Chen X-B, Chou WC (2020) Photocatalytic activity enhancement of Bi2WO6 nanoparticles by Ag doping and Ag nanoparticles modification. J Alloys Compd 824:153914. https://doi.org/10.1016/j.jallcom.2020.153914

Pouresmaeil H, Faramarz MG, ZamaniKherad M, Gheibi M, Fatollahi-Fard AM, Behzadian K, Tian G (2022) A decision support system for coagulation and flocculation processes using the adaptive neuro-fuzzy inference system. Int J Environ Sci Technol 19(10):10363–10374. https://doi.org/10.1007/s13762-021-03848-4

Seid-Mohammadi AS-M, Zolghadr Nasab H, Nouri F, Yavari D (2021) Efficiency of persulfate activated by uv irradiation in the presence of granular activated carbon for removal of methylene blue dye from aqueous solution. Sci J Kurdistan University Medical Sci 26(3):52–70

Senthil RA, Wu Y, Liu X, Pan J (2021) A facile synthesis of nano AgBr attached potato-like Ag2MoO4 composite as highly visible-light active photocatalyst for purification of industrial waste-water. Environ Poll 269:116034. https://doi.org/10.1016/j.envpol.2020.116034

Tran CV, La DD, Thi Hoai PN, Ninh HD, Thi Hong PN, Vu THT, Nadda AK, Nguyen XC, Nguyen DD, Ngo HH (2021) New TiO2-doped Cu–Mg spinel-ferrite-based photocatalyst for degrading highly toxic rhodamine B dye in wastewater. J Hazardous Mater 420:126636. https://doi.org/10.1016/j.jhazmat.2021.126636

Veziroglu S, Obermann A-L, Ullrich M, Hussain M, Kamp M, Kienle L, Leißner T, Rubahn H-G, Polonskyi O, Strunskus T, Fiutowski J, Es-Souni M, Adam J, Faupel F, Aktas OC (2020) Photodeposition of Au nanoclusters for enhanced photocatalytic dye degradation over TiO_2 thin film. ACS Appl Mater Interfaces 12(13):14983–14992. https://doi.org/10.1021/acsami.9b18817

Vinayagam R, Selvaraj R, Arivalagan P, Varadavenkatesan T (2020) Synthesis, characterization and photocatalytic dye degradation capability of Calliandra haematocephala-mediated zinc oxide nanoflowers. J Photochemistry Photobiol b: Biology 203:111760. https://doi.org/10.1016/j.jphotobiol.2019.111760

Yaseen DA, Scholz M (2019) Textile dye wastewater characteristics and constituents of synthetic effluents: a critical review. Int J Environ Sci Technol 16(2):1193–1226. https://doi.org/10.1007/s13762-018-2130-z

Zhao J, Liu J, Li N, Wang W, Nan J, Zhao Z, Cui F (2016) Highly efficient removal of bivalent heavy metals from aqueous systems by magnetic porous Fe3O4-MnO2: Adsorption behavior and process study. Chem Eng J 304:737–746. https://doi.org/10.1016/j.cej.2016.07.003